IOP PUBLISHING JOURNAL OF PHYSICS: CONDENSED MATTER
J. Phys.: Condens. Matter **24** (2012) 084007 (12pp) doi:10.1088/0953-8984/24/8/084007

Imaging and manipulation of adatoms on an alumina surface by noncontact atomic force microscopy

G H Simon, M Heyde and H-J Freund

Fritz-Haber-Institute of the Max-Planck-Society, Department of Chemical Physics, Faradayweg 4-6, 14195 Berlin, Germany

E-mail: heyde@fhi-berlin.mpg.de

Received 22 September 2011, in final form 4 November 2011
Published 7 February 2012
Online at stacks.iop.org/JPhysCM/24/084007

Abstract
Noncontact atomic force microscopy (NC-AFM) has been performed on an aluminum oxide film grown on NiAl(110) in ultrahigh vacuum (UHV) at low temperature (5 K). Results reproduce the topography of the structural model, unlike scanning tunnelling microscopy (STM) images. Equipped with this extraordinary contrast the network of extended defects, which stems from domain boundaries intersecting the film surface, can be analysed in atomic detail. The knowledge of occurring surface structures opens up the opportunity to determine adsorption sites of individual adsorbates on the alumina film. The level of difficulty for such imaging depends on the imaging characteristics of the substrate and the interaction which can be maintained above the adsorbate. Positions of single adsorbed gold atoms within the unit cell have been determined despite their easy removal at slightly higher interaction strength. Preliminary manipulation experiments indicate a pick-up process for the vanishing of the gold adatoms from the film surface.

(Some figures may appear in colour only in the online journal)

1. Introduction

Now that noncontact atomic force microscopy (NC-AFM), or frequency modulation dynamic force microscopy (FM-DFM) as we prefer to call it (see e.g. chapter 7 in [1]), has matured to the extent that more and more groups are moving into the field, parallels and striking differences to its forerunner, scanning tunnelling microscopy (STM), become obvious. Unique capabilities of NC-AFM have been presented [2–4] and combining methods and results of NC-AFM and STM seems more promising than ever. One field where this can be beneficial is the characterization and manipulation of individual atomic or molecular adsorbates on various ordered, defected or disordered surfaces. Dual-mode NC-AFM/STM can provide new impetus to single molecule physics and chemistry at surfaces even though NC-AFM and STM are slightly limited by effects related to the convolution of tip and surface shapes. So far force microscopy studies have mostly been performed on nanometre sized particles (a few nanometres to hundreds of nanometres) on various surfaces such as those of metals, semiconductors, bulk oxides and thin films. Individual adsorbed molecular or atomic entities, in contrast, have been studied in only a few cases, very recently, and only seldom have adsorbate and substrate been resolved simultaneously [5–9, 2, 10–14]. The latter is particularly difficult if the adsorbate moves easily in the tip–sample potential, an aspect NC-AFM again has in common with STM. However, schemes to overcome this issue in the case of STM have been presented and transferred to NC-AFM [15, 10].

In the following we present results on an aluminum oxide film surface which highlight the imaging capabilities of the NC-AFM method and its ability to characterize both the surface structure and its defects. This is then extended to the adsorption position of metal atoms. Furthermore, preliminary results on interaction of such an atom with the tip and its manipulation are shown.

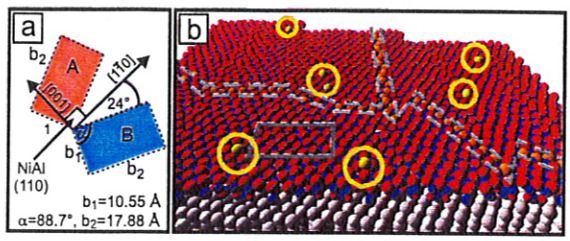

Figure 1. (a) Geometry of the alumina/NiAl(110) epitaxial relation. (b) Ball model of the ultrathin alumina/NiAl(110) surface including three antiphase domain boundaries of the defect network and their triple junction (large red and small blue balls for the oxide, boundary and junction sites in lighter colour between dashed lines, substrate Ni light grey and substrate Al larger and dark grey). Several adatoms (yellow, encircled) are shown as examples on a range of sites. A quadrangle marks the parallelogram shaped unit cell.

It is well established that oxidation of a clean (110) surface of the ordered intermetallic NiAl at about 550 K and subsequent crystallization around 1100 K produces a flat, smooth and excellently ordered aluminum oxide film. This ultrathin alumina/NiAl(110) is only 5 Å thick and has the lattice constants $b_1 = 10.55$ Å and $b_2 = 17.88$ Å with an enclosed angle $\alpha = 88.7°$, as determined by low-energy electron diffraction (LEED) [16, 17]. This is 16 times larger than the 2.89 Å × 4.08 Å rectangular cell of the substrate. With its point symmetry reduced towards NiAl(110) the film can grow in two reflection orientations (mirror domains A and B), where b_2 is rotated by $+24°$ and $-24°$ against NiAl[1$\bar{1}$0], respectively [17–19]. Figure 1 shows a schematic diagram of the epitaxial relation alongside a ball model based on [20] for film (B domain) and substrate as well as for a domain boundary triple junction within the film. Throughout the text the vectorial notation for the b_1 and b_2 lattice vectors is omitted to avoid cumbersome nomenclature. Considerations apply equally to both reflection domains. If no morphological constraints are present, the two orientations are equally likely [21, 22]. Irrespective of this, the partially pseudomorphic film is only commensurate along NiAl[1$\bar{1}$0] (row matching [23]) and incommensurate along NiAl[001]. This has important implications for surface studies of adsorbates. Despite, or because of, this, the ultrathin alumina film on NiAl(110) is an interesting sample system for the study of adsorbates. Its smooth growth with the tendency to increase the size of underlying terraces [21] and its limited thickness make it a convenient interlayer to partly decouple adsorbates from the metal substrate. By virtue of this decoupling layer it is for example possible to study molecular excited states which decay too fast if the adsorbate sits on metals [24]. The film structure's size, symmetry and partial pseudomorphic growth further induce a variety of different domain boundaries which produce a characteristic defect network in the film surface with interesting properties on its own [25–27]. With a much higher site density and much larger number of different sites than rock-salt structure surfaces have, but in the range of current experimental and theoretical methods, it can be used to study adsorbate properties as well as particular interactions between film, substrate and adsorbate [28–30].

Scanning tunnelling spectroscopy (STS) and contact potential difference (CPD) measurements, i.e. the STM and NC-AFM related spectroscopies, can be used to their full extent in particular if applied in direct combination using the same metallic tip as implemented in dual-mode setups.

2. Quick notes on the experimental setup

For this work NC-AFM in ultrahigh vacuum (UHV, pressure $p < 10^{-10}$ mbar) at cryogenic temperatures (5 K) was carried out employing a dual-mode sensor. Utilizing a quartz tuning fork setup the home-built sensor implements NC-AFM and STM with the same Pt/Ir tip. This allows recording of the two signals simultaneously but clearly separated from each other at the respective position on the sample [31–33]. Adsorbate deposition has been performed in the low temperature microscope compartment with a built-in low power evaporator [34].

3. Alumina films on other substrates

Besides alumina/NiAl(110) ultrathin epitaxial alumina films have been reported on about 20 other substrates. With no claim to be exhaustive these are alumina films on the (001), (110) and (111) faces of aluminum [35–37], NiAl [38–40, 17], Ni_3Al [41–49] and FeAl [50, 51], on Fe_3Al(110) [52], CoAl(100) [53, 54], γ-TiAl(111) [55–57], Cu–9% Al(111) [58, 59], decagonal AlCoNi [60] as well as icosahedral AlPdMn and AlCuFe quasicrystals [61–63], Ni(111) [64], Mo(100) and (110) [65], Ag(111) [66, 67], Ru(0001) [68–70], Ta(110) [71], Re(0001) [72, 73], Fe(110) [74] and furthermore on other films or as a buffer layer as alumina on Nb(110)/sapphire(0001) [75–77], NiAl/Ni(111), Ni_3Al/Ni(111) [78, 79], NiAl/Cu(111) [80], SiO_2/Si, Si(001)–H [81], SiO_2/Mo(100) [82] and in GaN/alumina/Si. Compilations of data and results on several of the systems can be found in [83–87]. Many more films exist, but are thicker (several nanometres or tens of nanometres) and often involve further components or polycrystalline substrates [88]. For most of the latter no LEED or STM data have been presented to give evidence of the high surface order that is so advantageous in atomic scale surface studies. Most remarkable, the disordered phases on aluminum single crystals and technologically interesting buffer layers on niobium left aside, are the crystalline alumina films on various facets of the ordered intermetallics. Single crystal surfaces of equivalent orientation produce qualitatively very similar epitaxial modes for the alumina. In some cases even the observed structures are close to being identical [51, 59]. This is found to be especially pronounced for the films on NiAl(110), Cu–9% Al(111) and FeAl(110) faces, and it appears as if such films also occur on thin NiAl films on Ni(111) [79] and even on Al containing quasicrystals [89, 61, 60]. This connection is interesting because the peculiar stoichiometry of alumina/NiAl(110) suggested that the structure of the film was a unique product

of the properties of both materials, especially regarding the stoichiometry and geometry of the surface cell. The latter, however, does not seem to have such a strong influence on the atomic structure. These two-dimensional alumina structures seem to be a more general phenomenon [87]. Ordered thin films related to other sesquioxides can be grown on the (110) and (100) faces of the B2 alloy CoGa (isostructural to NiAl). In the case of GaO_x/CoGa(110), LEED shows a nearly hexagonal arrangement and close to commensurate growth [90]. As several other sesquioxides also produce corundum bulk structures (V_2O_3, Cr_2O_3, α-Ga_2O_3, α-Fe_2O_3, Ti_2O_3, Rh_2O_3, Co_2O_3) and some amount of miscibility occurs among them, it would be interesting to further explore related two-dimensional systems with respect to their existence and mutual chemistry.

4. Imaging the surface structure of alumina on NiAl(110)

Despite the fact that current development in NC-AFM proceeds towards further applications beyond the imaging of clean or adsorbate covered surfaces, imaging is essential to all measurements in NC-AFM/STM studies, be it only to verify that a certain adsorbate position or tip status has not changed significantly. Double tips are much more easily identified in images than in $\Delta f(z)$ curves. Furthermore, images are at least one order of magnitude faster in their acquisition than two- or three-dimensional force field plots (force spectroscopy) from which corresponding images can be extracted. Most importantly, every observed image contrast is a manifestation of a particular force interaction between tip and sample. Therefore, any force analysis will eventually have to solve the image contrast and image contrasts in turn provide input for force analysis.

For better appreciation of the problem, figure 2 shows atomic resolution NC-AFM images of four different surfaces. An early high quality image of the well known Si(111)-(7 × 7) reconstruction is shown in comparison to the alumina film on $Ni_3Al(111)$, the $(\sqrt{31} \times \sqrt{31})R9°$ reconstructed α-$Al_2O_3(0001)$ surface and alumina/NiAl(110) [91, 48, 92–94, 20]. The frames show surface areas of identical size but very different site densities and contrasts and testify not only to the development in imaging over the years, but also the necessity for this development. In particular, the subtle and complex corrugations superposed onto the lateral positions of the alumina unit cells resemble more the corrugations found on strained metal layers than the smooth and spaciously arranged sites on {001} surfaces of rock-salt structures. The somewhat different contrast in the two middle images is due to a quasi-constant height recording in contrast to constant Δf recording in the two other frames. This emphasizes that image interpretation is non-trivial and requires a sound understanding of signal formation in the individual experimental implementation of NC-AFM.

In the case of alumina/NiAl(110) atomic resolution requires us to resolve a large number of inequivalent and closely spaced sites exhibiting subtle topographic features as well as more complicated structures which emerge at the film's extended defect network.

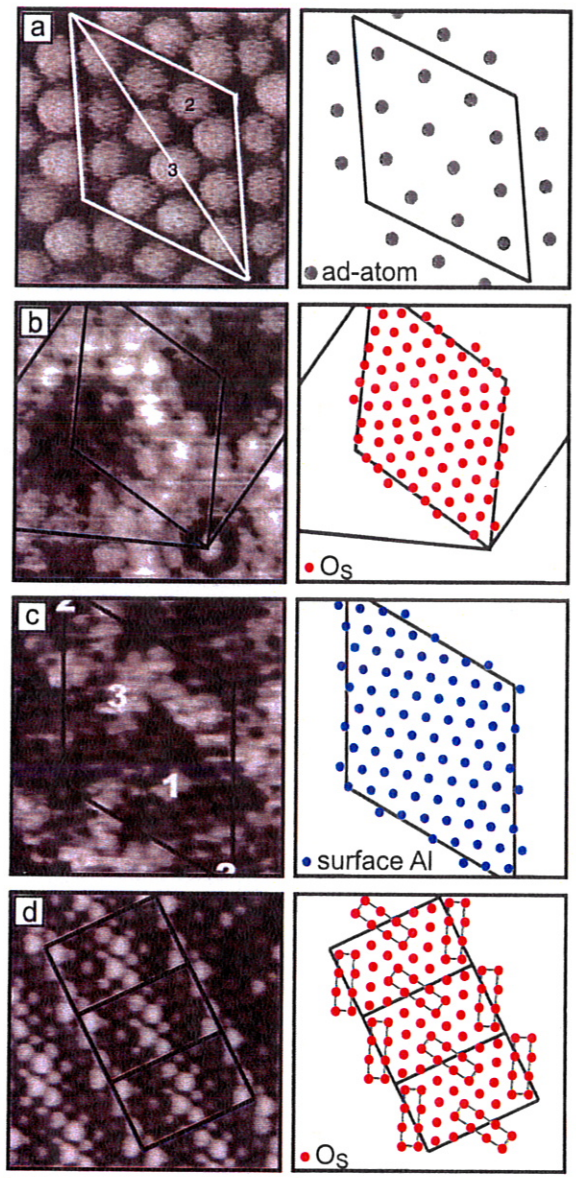

Figure 2. Comparison of an atomic resolution NC-AFM image of silicon with recent NC-AFM results from different alumina surfaces. Sizes: 4 nm × 4 nm. (a) Si(111)-(7 × 7) (reproduced with permission from [91]. Copyright 2001 AAAS), (b) alumina/$Ni_3Al(111)$ (reproduced with permission from [48]. Copyright 2007 American Chemical Society), (c) $Al_2O_3(0001)$-$(\sqrt{31} \times \sqrt{31})R9°$ (reproduced from [93]. Copyright 2009 American Physical Society) and (d) alumina/NiAl(110) [94]. Next to each image a model of the imaged sites is shown (citation for (b): [92]).

For (nominal) Pt/Ir tips on alumina/NiAl(110), experiments reveal a reproducible contrast mechanism. Atomic resolution can be obtained by scanning certain stable tip apices at a moderate attractive interaction with related frequency shifts usually in the range of -7 Hz $< \Delta f <$ -1 Hz. NC-AFM images, like the one in figure 2(d), show 28 protrusions in the unit cell at about 3 Å lateral separation, a number quite different from the 24 or 16 sites observed in certain STM contrasts [95, 96]. LEED data provide the framework for accurate identification of protrusions and determination of their fractional coordinates from images as

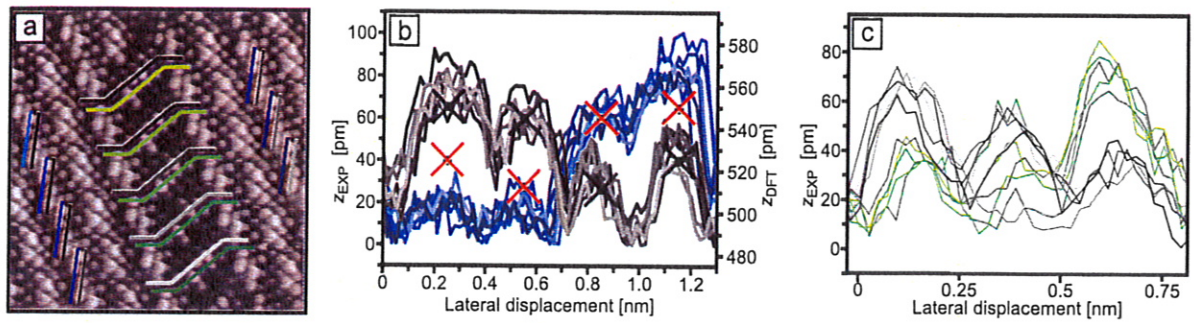

Figure 3. (a) High quality NC-AFM image of alumina B domains separated by an APDB I, which itself contains a lateral step defect at the top of the image. Scan size, 6.4 nm × 6.4 nm; sensor parameters, $\Delta f = -1.25$ Hz, $A_{OSC} = 3.8$ Å, $V_S = -200$ mV. (b), (c) Topographic contrast. (b) Comparison of corrugation for the rectangular block of eight O_S at an angle to NiAl[001] with that of the DFT model [20]. (c) Block of six O_S nearly perpendicular to the line vector of the boundary. See lines in corresponding colour and orientation in (a).

the measured lattice constants allow for correction of drift in NC-AFM and STM images.

Regarding the imaged species, some information was available prior to our NC-AFM studies. The film had been known to be reduced and to be composed of aluminum and oxygen layers with oxygen termination towards the vacuum. Combination of STM and DFT identified four layers in an $O_S/Al_S/O_i/Al_i$/NiAl(110) stacking [20].

The DFT model has a slightly broader unit cell ($b_1 = 10.93$ Å, $b_2 = 17.90$ Å, $\alpha = 88.16°$) to obtain a treatable commensurate arrangement for the computational supercell. A similar approach has been pursued in a subsequent DFT study concerning the simplest antiphase domain boundary (APDB) in the defect network of the film [97].

Notable in the proposed structure are the square and rectangular O_S arrangements at the surface (see green rectangles in figure 2(d)). The unit cell comprises these blocks of eight O_S in two orientations. Blocks of each type are connected by square structures into chains.

Lateral positions of sites in NC-AFM images like the one shown in figure 2(d) reproduce accurately the O_S layer of the model and are therefore identified as surface oxygen atoms. Resolution on this surface and in this contrast typically evolves as follows: first wave crests are resolved [98], followed by unit cell resolution, structural element resolution and eventual full atomic resolution of the entire O_S surface lattice. Other contrasts are either flawed (double tips) or do not give proper atomic resolution. They also occur much less frequently. Best obtainable resolutions for given tips are determined and limited by the chosen Δf setpoint, tip shape (double tip effects) and tip stability.

Another merit of this contrast lies in the confirmation of atomic corrugations within the model's surface structure. In figure 3 this is shown for two domains separated by the most ordered domain boundary type APDB I close to a lateral step defect within the boundary at the top of this image.

Line profiles taken across characteristic structural elements of the unit cell and of the type I APDB of this image are shown in subfigures 3(b) and (c) in comparison to the corrugation of the corresponding positions in the DFT model. This is a good real space and high resolution confirmation of important structural features in the DFT model and has been derived without prior assumptions regarding contrast formation. We therefore find NC-AFM to be the method of choice to analyse the fine details in surface topography on (oxide) surfaces like the ones shown in figure 2. Furthermore, the alumina surfaces therein can be considered benchmark systems for lateral and topographical resolution exceeding the requirements of, e.g., the Si(111)-(7 × 7) reconstruction or {001} surfaces of rock-salt structures.

While a full picture of contrast formation in all physical and chemical detail is not available at the current stage for metal tips on alumina/NiAl(110), the precise knowledge of the imaged species is a good starting point for an analysis of the force interaction. This is further supplemented by the good conductivity of the tip as confirmed by co-recorded tunnelling current (I_T).

Theory generally considers oxide terminated tips over oxide surfaces. This is based on the assumption that small oxide pieces will be picked up during scanning or residual native oxide of the tip material is present (see chapters 6 and 17 in [99]). For archetypical ionic oxides, imaging of one ion species at a time is usually observed. This leads directly to the open question of contrast inversion upon exchange of the terminating ion at the tip apex. While some results from MgO [100] back up this idea it may not be ionic attraction or repulsion which contributes most importantly to atomic scale NC-AFM contrast. This could be particularly true on partly covalent compounds like alumina and alumina films.

5. Domain boundaries within ultrathin alumina on NiAl(110)

Once an understanding of the observed NC-AFM contrast resulting from the structure has been gained, further details of the structure can be assessed from individual images if their quality suffices. For alumina/NiAl(110) the study of its defect network suggests itself. The network is produced by step edges and line defects created upon intersection of different types of domain boundaries with the film surface. Figure 4(a) gives an impression. The domain boundaries are due to the partial pseudomorphic epitaxy and boundaries of different origin will be present. Reflection domain boundaries (RDBs) parting oxide areas of different mirror orientations are the

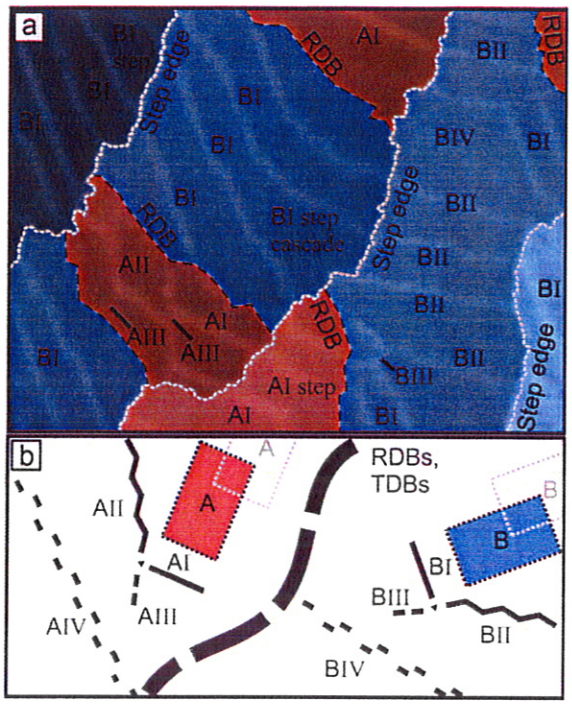

Figure 4. Domain boundary types. (a) STM overview scan ($I_T = 150$ pA, $V_S = 3.5$ V, scan area: 80 nm × 107 nm) showing the domain boundaries as bright protrusions. Nucleation related boundaries are not present, but would appear much like RDBs. Together with step edges the latter two form the perimeter of an oxide patch. APDBs form within such pristine film areas. (b) Sketch of the different domain boundary types and their orientations with respect to the oxide unit cells: APDBs I, II, III and IV as well as nucleation related TDBs and RDBs.

most obvious and so are translation related domain boundaries (TDBs) between oxide patches at lateral displacements compatible with the lattice of the substrate but not with that of the oxide. They delimit an oxide patch upon growth from the adsorbed amorphous oxygen precursor during crystallization, just as step edges can do. Of a more intriguing kind are strain relief related translation domain boundaries, so called antiphase domain boundaries (APDBs) [18, 101, 102, 95, 103, 97]. They exist within the just mentioned oxide patches and are introduced only after crystallization. Frequently, networks formed by APDBs are the most striking features in images of the film. The reproducibility in appearance of the defect network originates from preferred orientations of step edges and boundaries within the oxide and, related to this, recurring network motifs [18, 95, 94, 104]. Subfigure 4(b) describes these preferred orientations of the various domain boundary types within the oxide. However, it takes atomic scale images to determine the structural and topological nature, e.g. Burgers vector length and orientation, of the boundaries. One example is the APDB I in figure 3(a) with the onset of a step in the boundary path at the top of this image. Another is an elbow shaped path of two type I and II APDBs with a junction between them, which raises the question regarding a third type of APDB [95]: a structure necessary to produce unstrained junctions as suggested in figure 1.

A notable feature of the NC-AFM images of domain boundaries in alumina/NiAl(110) are the structural elements characteristic for the various boundary types. Typically they are derived from the rectangular blocks of 8 O_S sites or the square of 4 O_S atoms connecting these blocks into chains along the two alternating wave crests in the film topography. In figure 3 such a square is extended into a rectangle of six surface oxygens, confirming the DFT models which emphasized this kind of structural element [20, 97, 92]. The strain relief related APDBs are the most ordered defect structures while the numerous lateral displacements and boundary paths possible for nucleation related TDBs and RDBs suggest more variability. In particular, RDBs come in various orientations which change continuously along their path, as they can encircle entire oxide islands. APDBs in contrast grow so regularly that peculiar variations in topographic height can be observed among boundary segments with the same lateral structures. Their topography appears rotated by 180° in conformity with the oxide symmetry. It is speculated whether this is just related to residual strain in the topmost layer of the film or a manifestation of the local film–substrate relation. In the case of the latter NC-AFM could provide a unique opportunity to determine locally the film–substrate or adsorbate–substrate registry, a question which has complicated studies on individual adsorbates so far, mainly because the partial incommensurability will increase the number of qualitatively different adsorption sites beyond the numerous different top, bridge and hollow sites already existing in the unit cell. This is an important aspect when adsorbates interact not only with the alumina, but also with the NiAl substrate. It has for instance been shown that growth and charging of linear gold chains depends on the alignment of adsorbate, film and substrate sites [30, 105].

6. Adsorbed gold atoms on alumina on NiAl(110)

Having emerged on the background of model catalysis where the film has been used as a model support, adsorption onto the alumina/NiAl(110) surface has been extensively explored with averaging ensemble techniques. Table 1 lists published work on various species adsorbed directly onto the alumina film. Results on adsorption and reaction of molecules on metallic nanoparticles grown on the alumina film have been omitted therein for brevity. Most studies employed physical vapour deposition in UHV to provide clean adsorbate–film systems. More recently, the detailed knowledge of the film properties enabled microscopy and spectroscopy studies of individual atoms and molecules or molecular complexes on the alumina/NiAl(110) system. In particular Mn [28], Pd [106], Ag, Pt [107] and Au [30, 108, 10] adatoms as well as C_{60} [29, 109, 110], C_{70} [29], zinc(II)-etioporphyrin I (ZnEtioI) [111, 112], copper phthalocyanine (CuPc) [113, 96], magnesium porphine (MgP) [114–116], naphthalocyanine (NPc) [117, 118] and adsorbed vanadia species [119] have been characterized with respect to properties like adsorption behaviour and site, charging, wetting, vibrational modes or magnetism.

Metals evaporated onto alumina/NiAl(110) at room temperature usually form large aggregates [84]. Only

Table 1. Literature on adsorbates on alumina/NiAl(110).

Metals on alumina/NiAl(110)	
Al hydroxylated	[120, 102]
V	[121, 84]
Mn	[28]
Co	[122, 120, 84, 123–125]
Ni	[126]
Ge	[126]
Rh	[127]
Pd	[128, 125]
Ag	[129, 30]
Ta	[130]
Ir	[123]
Pt	[131, 132, 84, 107]
Au	[133, 105, 108, 10]
Alloys on alumina/NiAl(110)	
AgAu	[133]
PdCo	[125]
Compounds on alumina/NiAl(110)	
NiO	[126]
BaO	[134]
Ferria	[135]
Niobia	[136]
Vanadia	[137, 119]
[BMIM][Tf_2N] (ionic liquid)	[138, 139]
Molecules on alumina/NiAl(110)	
CO	[140, 24, 141]
CO_2	[140]
O_2	[140, 24]
NO	[140, 25]
NO_2	[142]
H_2O	[140]
D_2O	[143]
Methanol	[144]
C_{60}	[29, 145]
C_{70}	[29]
Alkali metals/C_{60}	[110]
Ag/C_{60}	[109]
$Rh(OAc)_2$	[146]
$RhCl_3$	[146]
Di-tert-butyl nitroxide	[147, 148]
Zinc(II) etioporphyrin I (ZnEtioI)	[111, 112]
Copper phthalocyanine (CuPc)	[113, 96]
Magnesium porphine (MgP)	[114–116]
Naphthalocyanine (NPc)	[117, 118]
Trans-1,2-dichloroethene/Cu	[149]

evaporation onto a cooled film surface (~10 K) at low coverages produces single adatoms and small nuclei that are distributed across the surface. In setups similar to ours this can be conveniently done with built-in or portable low power evaporators (micro-evaporators) [34]. Stabilization of linear nuclei has been found on such preparations at slightly higher coverage and the electronic structure as well as the charge state of single adatoms or chains has been explored [106, 30, 105, 108]. However, analysis in such endeavours is limited by the large number of possible adsorption sites provided by the alumina unit cell and an even larger number if the boundaries play a role as in the case of palladium, which shows a preference for nucleation at the defect network. In addition, the incommensurability poses a complication in binding site determination in the specific case of alumina/NiAl(110). Due to this, equivalent surface sites may not be identical binding sites if the underlying NiAl substrate has an influence. The latter has been shown for adsorbed gold [105]. NC-AFM can also master this hurdle, although such studies are a bit cumbersome [10]. The main reason is motions of the adsorbed species as easily induced by the (scanning) tip. Figure 5(a) shows an overview image of adsorbed gold atoms on the alumina film surface. Subfigures 5(b) and (c) show an NC-AFM image of a single atom. As in STM, the Pt/Ir tip images an adsorbed gold atom as a circular protrusion with bell-shaped height profile. It also appears larger than expected from a single atom even though the tip trajectory is already closer to the surface in NC-AFM than in STM. The latter is assessable from the co-recorded tunnelling current at the set bias voltage in our dual-mode images. As motion of the adsorbate within (e.g. sideways bending) or away from its binding site has to be avoided, the interaction has to be adjusted accordingly. Inferring the substrate structure from the atomically resolved substrate nearby and taking the adsorption bond to be at the centre of the bell-shaped protrusion of the gold atom, one obtains the adsorption position of the adatom. A vertical bond is also the outcome of DFT calculations [105]. In figures 6(a)–(c) the case of an atom moving on its site under the action of the tip is shown. The displacement becomes obvious under comparison of adatom positions in forward and backward scans. An altered setpoint reduced the interaction. Note that the tip changed slightly between the recordings and gave generally higher Δf in the last frame. As figure 5(b) shows, this may result in frequency shift (Δf) setpoints giving no resolution on the substrate. In such a case only a measurement protocol that changes the imaging parameters above the adspecies allows determination of its adsorption site. This has been done in the shown image. Such schemes have also been implemented by other groups for the identical reason of motion of the adsorbate [14]. Whether this is necessary and how adsorbate binding strength and experimental factors like sensitivity and setpoint affect this, may be assessed from an analysis of frequency shift–distance ($\Delta f(z)$) curves. Figure 7 compares a curve taken above a gold atom with another one taken on the alumina film underneath at a distance to the side of it. Both were recorded with the same tip apex. The two curves reflect not only the topography of the adatom being placed at higher z than the alumina underneath, but also a change in interaction strength between the two. Obtainable Δf values for the film surface had typically at least twice the values allowed on gold adatoms just before they would move. Atomic features of the alumina surface only become visible in the lower third of the $\Delta f(z)$ curve while curves above gold atoms always have their minimum above that and around 1 Hz.

Moving the tip towards the adatom one reaches—still on the attractive branch of the interaction curve—the onset of repulsion. This increases the energy of the

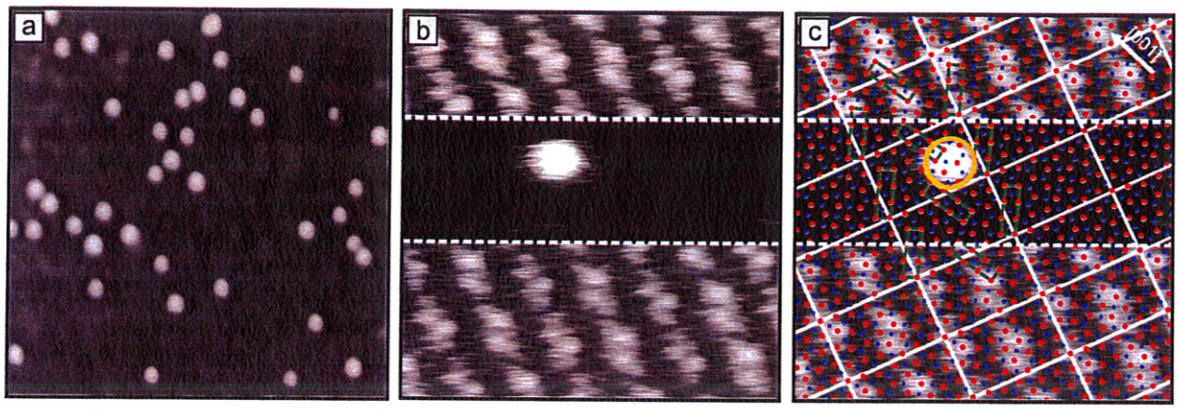

Figure 5. (a) STM image of gold atoms adsorbed onto the cold alumina/NiAl(110) surface. Scan area: 27 nm × 27 nm. $I_T = +50$ pA, $V_S = +1$ V. (b) NC-AFM image of an adsorbed gold atom on alumina/NiAl(110). Atomic resolution has been obtained before and after the tip approached the atom. The tip has been retracted above it. (c) The same image with the positioned model structure. The large yellow circle indicates the position of the adatom. Scan area: 6.4 nm × 6.4 nm, $\Delta f = -1.5$ Hz (-0.9 Hz above the Au adatom), $A_{OSC} = 3.8$ Å, $V_S = -200$ mV.

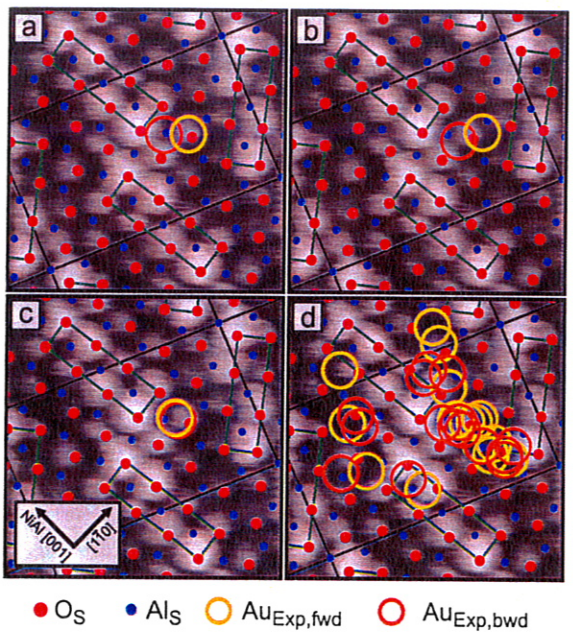

Figure 6. (a)–(c) Gold adatom positions from a series of three images. In the first two the adatom position differs between the forward and the backward scan while in the third image they are identical. $\Delta f = -1.50$, -1.50 and -1.58 Hz (-0.9, -0.93 and -0.93 Hz above the Au adatom). $A_{OSC} = 3.8$ Å, $V_S = -200$ mV. (d) All observed sites (forward and backward scans) for Au adatoms on both reflection domains mapped into one oxide unit cell. Sizes: 2 nm × 2 nm.

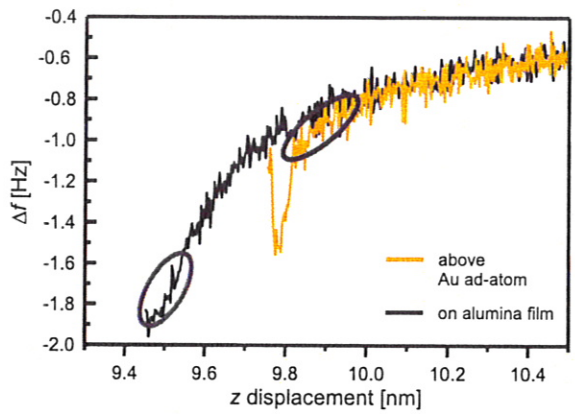

Figure 7. Two $\Delta f(z)$ curves recorded atop an adsorbed gold adatom and, with the same tip apex, on the alumina/NiAl(110) surface at some lateral distance to surrounding adatoms. $A_{OSC} = 3.8$ Å, $V_S = -300$ mV.

adatom until it eventually crosses some confining potential energy barrier. Consequently, curves above the gold atoms frequently show spike-shaped features instead of a shallow minimum. This is interpreted as a rapid structural change in the tip–adsorbate–alumina gap. At such comparably weak interaction it is most likely the adatom which changes its position. In fact it has been removed in this case. This could be by pushing it aside, or, more likely, by adsorption to the tip.

In part the difference between the curves will be simply due to a proximity effect. Above the protruding adsorbate only the latter shares interaction at small separation with the tip while many more atoms interact at comparable separation if the tip approaches the alumina surface. Nevertheless, a second part will inevitably reflect the different chemical nature and strength of the interaction between tip and adsorbate as compared to the oxide surface underneath. To further qualify the previous statement about experimental and sample system inherent limitations to the simultaneous resolution of adsorbate and substrate we consider the schematic $\Delta f(z)$ curves in figure 8.

Therein subfigures (a) and (b) show two different scenarios, each for two adsorbates with different interaction, i.e. different $\Delta f(z)$, curves. The first scenario in subfigure 8(a) assumes the surface to exhibit only one $\Delta f(z)$ curve which is shifted in z between different atomic sites. Therefore, it is possible to resolve the surface atomic structure in the full Δf range between the minimum and some value near 0 Hz determined by the noise of the experimental setup (Δf ranges marked in light and dark grey respectively). Considering now the simultaneous resolution of each of the adsorbate

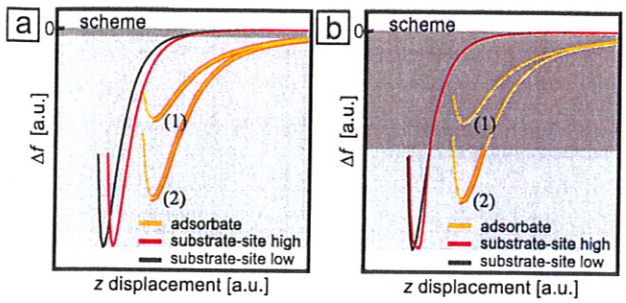

Figure 8. Schematic of two scenarios for the assessment of simultaneous NC-AFM adsorbate–substrate resolution for different adspecies (1) and (2). (a) Substrate resolvable over entire Δf range between 0 Hz and the minimum Δf value. Adsorbates can be resolved simultaneously with Δf setpoints down to the minimum of the adsorbate curve (bold line segments in $\Delta f\,(z)_{(1)}$ and $\Delta f\,(z)_{(2)}$). (b) Substrate only resolvable for Δf below some branching point. Only adsorbates sharing common Δf values with the substrate below that branching point can be resolved simultaneously with it (bold line segment in $\Delta f\,(z)_{(2)}$).

species (1) and (2) with the substrate it is clear that this is only attainable where common Δf values with the substrate exist (marked bold on the two adsorbate $\Delta f(z)$ curves) with the aforementioned experimental limitations. The Δf range covers both curves down to the minimum. In this case both adsorbates can be easily resolved together with the substrate. For setpoints in the light grey region below the minimum of an adsorbate curve, the respective adsorbate would be moved or picked up. Scenario (a) seems to be realized on surfaces like KBr and MgO [150, 32].

In scenario (b) (see figure 8(b)) the substrate $\Delta f(z)$ curves look entirely different. They lie on top of each other (Δf range marked again in dark grey) until a branching point is reached. Only below this point may the substrate surface be resolved (light grey). Hence, simultaneous resolution of adsorbate and surface sensitively depends on the relative depth of the adsorbate and substrate $\Delta f(z)$ curves. This is an important difference from scenario (a). For adsorbate (1) all Δf values lie above the branching point of the substrate curves. Only the adsorbate can be imaged in this case. Adsorbate (2), in contrast, can also be imaged at values allowing resolution of the substrate structure (Δf range marked with bold line segment). In the Δf range below the minimum of each adsorbate curves the respective adspecies gets again removed from its site.

The presented NC-AFM experiment on single gold atoms shows no resemblance with scenario (a), but with adsorbate (1) in scenario (b). This is clear from figures 5 and 7. On the alumina film $\Delta f(z)$ curves are typically found (at the sensor parameters in use) to produce detectable z-displacement between neighbouring sites in the lower third of the $\Delta f(z)$ curve. Furthermore, their branching point is already lower than the minimum value of curves obtained on Au adatoms. We therefore believe that under these circumstances simultaneous resolution of gold atoms on alumina/NiAl(110) is inherently impossible.

As claimed at the beginning of this section, weakly bound adatoms can be imaged in such a way that the substrate is resolved to an extent which allows determination of the atomic scale registry between both of them. As shown in figure 5, the trick is to retract the tip above the adatom [15]. For this purpose the substrate has to be imaged with atomic resolution at some point within the image before the tip is retracted to allow imaging of the adsorbate at weaker interaction conditions. It is clear that large imaged substrate areas preferably on both sides of the adsorbate give the best results, in particular if drift is present or domain boundaries interrupt the lattice.

This procedure has been successfully performed for a series of individual gold atoms on both reflection domains of the alumina film. The results are summarized in 6(c).

It becomes clear that there is no single adsorption site. Adsorbed gold has rather been found at various sites throughout the oxide unit cell. One likely reason for this result is the interaction of gold atoms not only with the alumina film, but also with the NiAl(110) substrate underneath. Changing registry with the substrate for the individual unit cells due to the partial incommensurate growth alters the local adsorption properties, an aspect not fully captured in DFT calculations. Underlaying the positions with an NC-AFM image of the alumina/NiAl(110) unit cell visualizes the accumulation of adsorption positions between the wave crests of the oxide's O_S layer. A few sit on the wave crests and none have been found on the centres of the structural elements (green rectangles) or the square O_S groups connecting them. This behaviour is found to be reproduced in the distribution of special adsorption obtained by DFT calculations [105, 10]. Therein adsorption has been calculated to be especially strong if an Al_S is underneath the gold atom and in vertical alignment with an additional aluminum position in the substrate, but other sites allow binding as well.

It may be speculated that the wave-like topography of the oxide film affects the motion of adsorbates in favour of lower lying sites.

Imaging of easily movable adsorbates such as gold adatoms on alumina/NiAl(110) directly suggests further study of the interaction between tip and adsorbate up to and beyond the point of their manipulation. Figure 9 therefore shows preliminary results for future manipulation experiments. Different from the proceedings in [9, 2], which used constant height and point-wise measurements to determine the interaction above adsorbates, the tip has been controlled to constant Δf setpoint while scanning back and forth across a gold adatom. Between scans the setpoint has been successively lowered from -900 to $-1,210$ mHz until the signal from the adatom eventually vanishes. The last scan line is found to be shifted by $\sim$15 pm to larger distance towards the sample surface. From the successively recorded data it is possible to extract $\Delta f(z)$ curves. Such discrete curves have been found to be in good agreement with curves measured prior to the manipulation experiment in a continuous sweep (not shown here). Hence we find the validity of our implicit assumption confirmed, that a series of line scans at constant Δf can be used to represent details of the interaction between tip and adsorbate. This is in line with the findings in [151], but drift played a minor role in our

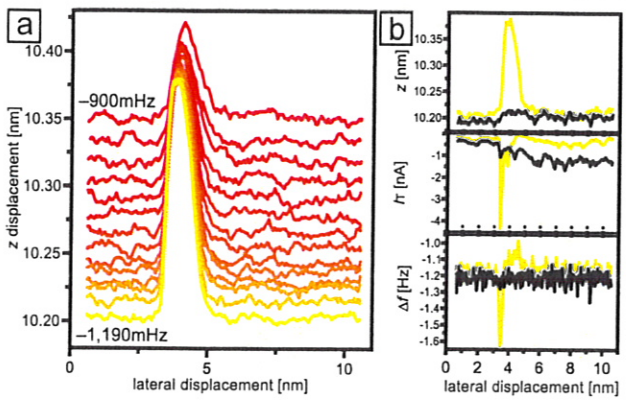

Figure 9. Line scans across a single adsorbed gold atom on alumina/NiAl(110) at increasing interaction strength. (a) Each line is averaged over six forward scans at fixed Δf (backward scans not shown). Eventually the adatom is removed from its site at $\Delta f = -1,210$ mHz. $A_{OSC} = 3.8$ Å, $V_S = -300$ mV. (b) Event of adatom removal in the respective consecutive single line scans (not averaged). Removal takes place in the data set marked in black. Shown are signals from the simultaneously recorded topography, current and frequency shift channels (z, I_T, Δf).

smaller dataset. Considering that gold can acquire negative charge on the alumina/NiAl(110) and assuming that even an uncharged gold atom might produce a minute electric dipole moment upon adsorption on the alumina film above the metallic substrate, the applied negative bias would attract (repel) the adatom into (out of) the tip–sample gap in the case of negative (positive) charge on the adsorbate. As no accumulation outside the scan frame has been observed after NC-AFM imaging of the alumina substrate, it is concluded that the gold is dragged into the gap and picked up by the scanning tip. A possible interpretation refers to a particle confined between two different approaching plates. To each of them it binds if brought close to it. This binding will differ in strength. Initially bound to one plate (i.e. the alumina/NiAl(110) surface), the particle (gold adatom) is situated in a double well potential. It rests near the surface until the well closer to the tip is getting more favourable upon tip approach. At $\Delta f = -1.21$ Hz, the oscillating tip seems to lower the barrier between the wells sufficiently that the gold moves to the tip. The well at the tip has to be deeper than that at the gold binding site on the alumina. Consequently, the atom stays at the tip afterwards.

Taking this picture a bit further, the oscillation of the tip constitutes attempts along the reaction coordinate against the mentioned barrier. If thermal vibrations were eliminated, as possible to some extent at even lower temperatures (<1 K), it may be possible to gain kinetic information through such experiments. Again, the tunnelling current could be used to monitor the time response.

7. Conclusion

With our dual-mode noncontact atomic force and scanning tunnelling microscopy (NC-AFM or FM-DFM and STM) experiments we have demonstrated state of the art imaging of an alumina/NiAl(110) film surface with high surface oxygen site density and subtle topographic features. This includes imaging of extended surface defects appearing where the film's various domain boundaries intersect its surface. Further, it has been shown that this very basic prerequisite of imaging is challenged already by simple adsorbates such as single gold adatoms on this surface. It appears that no common frequency shift (Δf) setpoint exists and simultaneous resolution of gold atoms and the alumina surface is prohibited. The reason for this is the shallow $\Delta f(z)$ curve above the gold atoms, which does not extend into the range where the alumina surface can be resolved. In consequence, gold atoms can easily be removed from their adsorption sites. While being inconvenient, this limitation to imaging some adsorbate species can be circumvented by appropriate measurement protocols. In fact, such adsorbates may be archetypical for certain manipulation/pick-up experiments. To this end preliminary results for manipulation have been shown. In particular, we have used scans across a gold adatom at constant Δf to monitor the interaction until the point where the adatom is displaced.

Presented results point out the excellent contributions NC-AFM constant Δf imaging provides in dual-mode NC-AFM/STM studies. It is concluded that the capabilities of NC-AFM are used most effectively on metal supported film systems, which allow STM to be performed alongside NC-AFM. Only this enables direct comparison of tunnelling and force related data. At the same time the use of a metal tip should be beneficial for potential control and therefore control of electrostatic background forces.

References

[1] Morita S, Giessibl F J and Wiesendanger R (ed) 2009 *Noncontact Atomic Force Microscopy* (*Springer Series Nanoscience and Technology*) vol 2 (Berlin: Springer)
[2] Gross L, Mohn F, Moll N, Liljeroth P and Meyer G 2009 *Science* **325** 1110–4
[3] König T, Simon G H, Rust H-P, Pacchioni G, Heyde M and Freund H-J 2009 *J. Am. Chem. Soc.* **131** 17544–5
[4] Sweetman A, Jarvis S, Danza R, Bamidele J, Gangopadhyay S, Shaw G A, Kantorovich L and Moriarty Ph 2011 *Phys. Rev. Lett.* **106** 136101
[5] Oyabu N, Sugimoto Y, Abe M, Custance Ó and Morita S 2005 *Nanotechnology* **16** S112
[6] Lauritsen J V, Foster A S, Olesen G H, Christensen M C, Kühnle A, Helveg S, Rostrup-Nielsen J R, Clausen B S, Reichling M and Besenbacher F 2006 *Nanotechnology* **17** 3436–41
[7] Gritschneder S and Reichling M 2007 *Nanotechnology* **18** 044024
[8] Gritschneder S, Iwasawa Y and Reichling M 2007 *Nanotechnology* **18** 044025
[9] Ternes M, Lutz C P, Hirjibehedin C F, Giessibl F J and Heinrich A J 2009 *Science* **319** 1066–9
[10] Simon G H, König T, Rust H-P, Ganduglia-Pirovanov M V, Sauer J, Heyde M and Freund H-J 2010 *Phys. Rev.* B **81** 073411
[11] Lämmle K, Trevethan Th, Schwarz A, Watkins M, Shluger A and Wiesendanger R 2010 *Nano Lett.* **10** 2965–71
[12] Gross L, Mohn F, Moll N, Meyer G, Ebel R, Abdel-Mageed W M and Jaspars M 2010 *Nat. Chem.* **2** 821–5

[13] Guillermet O, Gauthier S, Joachim Ch, de Mendoza P, Lauterbach Th and Echavarren A 2011 *Chem. Phys. Lett.* **511** 482–5

[14] Mohn F, Gross L and Meyer G 2011 *Appl. Phys. Lett.* **99** 053106

[15] Doering M, Buisset J, Rust H-P, Briner B G and Bradshaw A M 1996 *Faraday Discuss.* **105** 163–75

[16] Müller K, Lindner H, Zehner D M and Ownby G 1990 *Verh. Dtsch. Phys. Ges.* **25** 1130

[17] Jaeger R M, Kuhlenbeck H, Freund H-J, Wuttig M, Hoffmann W, Franchy R and Ibach H 1991 *Surf. Sci.* **259** 235

[18] Libuda J, Winkelmann F, Bäumer M, Freund H-J, Bertrams Th, Neddermeyer H and Müller K 1994 *Surf. Sci.* **318** 61–73

[19] Libuda J 1996 Die Struktur von Trägerkatalysator-Modellsystemen auf geordneten Oxidfilmen *PhD Thesis* Universität Bochum

[20] Kresse G, Schmid M, Napetschnig E, Shishkin M, Köhler L and Varga P 2005 *Science* **308** 1440–2

[21] Ulrich S, Nilius N and Freund H-J 2007 *Surf. Sci.* **601** 4603–7

[22] Ellinger C, Vonk V, Khorshidi N, Vlad A, Stierle A and Dosch H 2009 *New J. Phys.* **11** 113004

[23] Stierle A, Renner F, Streitel R, Dosch H, Drube W and Cowie B C 2004 *Science* **303** 1652–6

[24] Jaeger R M, Libuda J, Bäumer M, Homann K, Kuhlenbeck H and Freund H-J 1993 *J. Electron Spectrosc. Relat. Phenom.* **64/65** 217–25

[25] Schauermann S, Johánek V, Laurin M, Libuda J and Freund H-J 2003 *Chem. Phys. Lett.* **381** 298–305

[26] Nilius N, Kulawik M, Rust H-P and Freund H-J 2004 *Phys. Rev.* B **69** 121401(R)

[27] Heinke L, Lichtenstein L, Simon G H, König T, Heyde M and Freund H-J 2010 *ChemPhysChem* **11** 2085–7

[28] Heinrich A J, Gupta J A, Lutz C P and Eigler D M 2004 *Science* **306** 466–9

[29] Liu N, Pradhan N A and Ho W 2004 *J. Chem. Phys.* **120** 11371–5

[30] Kulawik M, Nilius N and Freund H-J 2006 *Phys. Rev. Lett.* **96** 036103

[31] Heyde M, Sterrer M, Rust H-P and Freund H-J 2005 *Appl. Phys. Lett.* **87** 083104

[32] Heyde M, Simon G H, Rust H-P and Freund H-J 2006 *Appl. Phys. Lett.* **89** 263107

[33] Rust H-P, Heyde M and Freund H-J 2006 *Rev. Sci. Instrum.* **77** 043710

[34] Rust H-P, König T, Simon G H, Nowicki M, Simic-Milosevic V, Thielsch G, Heyde M and Freund H-J 2009 *Rev. Sci. Instrum.* **80** 113705

[35] Belton D N and Schmieg S J 1988 *Appl. Surf. Sci.* **32** 173–92

[36] Erskine J L and Strong R L 1982 *Phys. Rev.* B **25** 5547–50

[37] Crowell J E, Chen J G and Yates J T Jr 1986 *Surf. Sci.* **165** 37–64

[38] Gaßmann P, Franchy R and Ibach H 1993 *J. Electron Spectrosc. Relat. Phenom.* **64/65** 315–20

[39] Blum R-P and Niehus H 1998 *Appl. Phys.* A **66** S529–33

[40] Franchy R, Masuch J and Gassmann P 1996 *Appl. Surf. Sci.* **93** 317–27

[41] Bardi U, Atrei A and Rovida G 1992 *Surf. Sci.* **268** 87–97

[42] Podgursky V, Costina I and Franchy R 2003 *Appl. Surf. Sci.* **206** 29–36

[43] Kurnosikov O, Flipse C F J, Swagten H J M, Koopmanns B and de Jonge W J M 2006 *Surf. Sci.* **600** 4375–9

[44] Cotterill G F, Niehus H and O'Connor D J 1996 *Surf. Rev. Lett.* **3** 1355–63

[45] Garza M, Magtoto N P and Kelber J A 2002 *Surf. Sci.* **519** 259–68

[46] Becker C, Kandler J, Raaf H, Linke R, Pelster T, Dräger M, Tanemura M and Wandelt K 1998 *J. Vac. Sci. Technol.* A **16** 1000–5

[47] Degen S, Krupski A, Kralj M, Langner A, Becker C, Sokolowski M and Wandelt K 2005 *Surf. Sci.* **576** L57–64

[48] Gritschneder S, Becker C, Wandelt K and Reichling M 2007 *J. Am. Chem. Soc.* **129** 4925–8

[49] Gritschneder S, Degen S, Becker C, Wandelt K and Reichling M 2007 *Phys. Rev.* B **76** 014123

[50] Graupner H, Hammer L, Heinz K and Zehner D M 1997 *Surf. Sci.* **380** 335–51

[51] Kizilkaya O, Hite D A, Zehner D M and Sprunger P T 2003 *Surf. Sci.* **529** 223–30

[52] Vonk V, Ellinger C, Khorshidi N, Vlad A, Stierle A and Dosch H 2008 *Phys. Rev.* B **78** 165426

[53] Podgursky V, Rose V, Costina J and Franchy R 2006 *Appl. Surf. Sci.* **252** 8394–8

[54] Podgursky V, Rose V, Costina J and Franchy R 2006 *Appl. Surf. Sci.* **253** 1796–800

[55] Maurice V, Despert G, Zanna S, Bacos M-P and Marcus P 2004 *Nature Mater.* **3** 687–91

[56] Maurice V, Despert G, Zanna S, Josso P, Bacos M-P and Marcus P 2005 *Surf. Sci.* **596** 61–73

[57] Li H, Wang S Q and Ye H Q 2009 *J. Mater. Sci. Technol.* **25** 569–76

[58] Yoshitake M, Bera S, Yamauchi Y and Song W 2003 *J. Vac. Sci. Technol.* A **21** 1290–3

[59] Napetschnig E, Schmid M and Varga P 2008 *Surf. Sci.* **602** 1750

[60] Burkardt S, Erbudak M and Mäder R 2009 *Surf. Sci.* **603** 867–72

[61] Burkardt S and Erbudak M 2009 *Surf. Sci.* **603** 2248–53

[62] Gil-Gavatz M, Rouxel D, Pigeat P, Weber B and Dubois J-M 2000 *Phil. Mag.* A **80** 2083–97

[63] Rouxel D and Pigeat P 2006 *Prog. Surf. Sci.* **81** 488–514

[64] Nemšák S, Skála T, Yoshitake M, Tsud N, Kim T, Yagyua S and Matolin V 2010 *Surf. Interface Anal.* **42** 1581–4

[65] Rainer D R, Xu C, Holmblad P M and Goodman D W 1997 *J. Vac. Sci. Technol.* A **15** 1653–62

[66] Oughaddou H, Vizzini S, Aufray B, Ealet B, Gay J-M, Bibérian J-P and d'Avitaya F A 2006 *Appl. Surf. Sci.* **252** 4167–70

[67] Vizzini S, Oughaddou H, Hoarau J Y, Bibérian J-P and Aufray B 2009 *Appl. Phys. Lett.* **95** 173111

[68] Frederick B G, Apai G and Rhodin T N 1991 *Surf. Sci.* **244** 67–80

[69] Frederick B G, Apai G and Rhodin T N 1991 *Phys. Rev.* B **44** 1880–90

[70] Wu Y, Tao H-S, Garfunkel E, Madey T E and Shinn N D 1995 *Surf. Sci.* **336** 123–39

[71] Chen P J and Goodman D W 1994 *Surf. Sci.* **312** L767–73

[72] Wu Y, Garfunkel E and Madey T E 1996 *Surf. Sci.* **365** 337–52

[73] Lai X, Chusuei C C, Luo K, Guo Q and Goodman D W 2000 *Chem. Phys. Lett.* **330** 226–30

[74] Dedkov Yu S and Fonin M 2007 *Appl. Surf. Sci.* **253** 3860–4

[75] Mašek K, Kapsa R and Matolín V 1998 *Surf. Sci.* **417** 139–44

[76] Dietrich Ch, Koslowski B and Ziemann P 2005 *J. Appl. Phys.* **97** 083515

[77] Welander P B and Eckstein J N 2007 *Appl. Phys. Lett.* **90** 243510

[78] Le Pévédic S, Schmaus D and Cohen C 2007 *Surf. Sci.* **601** 395–410

[79] Le Pévédic S, Schmaus D and Cohen C 2008 *Surf. Sci.* **602** 67–76

[80] Jeliazova Y and Franchy R 2002 *Appl. Surf. Sci.* **187** 51–9

[81] Vizzini S *et al* 2007 *J. Cryst. Growth* **305** 26–9
[82] Gründling Ch, Lercher J A and Goodman D W 1994 *Surf. Sci.* **318** 97–103
[83] Henry C R 1998 *Surf. Sci. Rep.* **31** 231–325
[84] Bäumer M and Freund H-J 1999 *Prog. Surf. Sci.* **61** 127–98
[85] Franchy R 2000 *Surf. Sci. Rep.* **38** 195–294
[86] Wu Q-H, Fortunelli A and Granozzi G 2009 *Int. Rev. Phys. Chem.* **28** 517–76
[87] Prévot G, Naitabdi A, Bernard R and Borensztein Y 2010 *Phys. Rev.* B **81** 085405
[88] Panda E, Jeurgens L P H and Mittemeijer E J 2010 *Surf. Sci.* **604** 588–95
[89] Burkardt S, Deloudi S, Erbudak M, Kortan A R, Mungan M and Steurer W 2008 *J. Phys.: Condens. Matter* **20** 314006
[90] März A and Franchy R 2000 *Surf. Sci.* **466** 54–65
[91] Lantz M A, Hug H J, Hoffmann R, van Schendel P J A, Kappenberger P, Martin S, Baratoff A and Güntherodt H-J 2001 *Science* **291** 2580–3
[92] Schmid M, Kresse G, Buchsbaum A, Napetschnig E, Gritschneder S, Reichling M and Varga P 2007 *Phys. Rev. Lett.* **99** 196104
[93] Lauritsen J V, Jensen M C R, Venkataramani K, Hinnemann B, Helveg S, Clausen B S and Besenbacher F 2009 *Phys. Rev. Lett.* **103** 076103
[94] Simon G H, König T, Rust H-P, Heyde M and Freund H-J 2009 *New J. Phys.* **11** 093009
[95] Kulawik M, Nilius N, Rust H-P and Freund H-J 2003 *Phys. Rev. Lett.* **91** 256101
[96] Mikaelian G, Ogawa N, Tu X W and Ho W 2006 *J. Chem. Phys.* **124** 131101
[97] Schmid M, Shishkin M, Kresse G, Napetschnig E, Varga P, Kulawik M, Nilius N, Rust H-P and Freund H-J 2006 *Phys. Rev. Lett.* **97** 046101
[98] Pang C L, Raza H, Haycock S A and Thornton G 2002 *Phys. Rev.* B **65** 201401(R)
[99] Morita S, Wiesendanger R and Meyer E (ed) 2002 *Noncontact Atomic Force Microscopy* (*Springer Series Nanoscience and Technology*) (Berlin: Springer)
[100] Shluger A L, Rohl A L, Williams R T and Wilson R M 1995 *Phys. Rev.* B **52** 11398–411
[101] Hansen K H, Worren T, Laegsgaard E, Besenbacher F and Stensgaard I 2001 *Surf. Sci.* **475** 96–102
[102] Heemeier M 2005 Morphologie und Wachstum von Übergangsmetallclustern auf modifizierten und unveränderten ultradünnen Oxidfilmen *PhD Thesis* Freie Universität Berlin
[103] McCarty K F, Pierce J P and Carter B 2006 *Appl. Phys. Lett.* **88** 141902
[104] Heinke L, Lichtenstein L, Simon G H, König T, Heyde M and Freund H-J 2010 *Phys. Rev.* B **82** 075430
[105] Nilius N, Ganduglia-Pirovano M V, Brázdová V, Kulawik M, Sauer J and Freund H-J 2008 *Phys. Rev. Lett.* **100** 095802
[106] Nilius N, Wallis T M and Ho W 2003 *Phys. Rev. Lett.* **90** 046808
[107] Cörper A, Bozdech G, Ernst N, Klüner T and Freund H-J 2005 *Phys. Status Solidi* b **242** 2462–7
[108] Nilius N, Ganduglia-Pirovano M V, Brázdová V, Kulawik M, Sauer J and Freund H-J 2010 *Phys. Rev.* B **81** 045422
[109] Nazin G V, Qiu X H and Ho W 2005 *J. Chem. Phys.* **122** 181105
[110] Pradhan N A, Liu N, Silien C and Ho W 2005 *Phys. Rev. Lett.* **94** 076801
[111] Qiu X H, Nazin G V and Ho W 2003 *Science* **299** 542–6
[112] Lee H J, Lee J H and Ho W 2005 *ChemPhysChem* **6** 971–5
[113] Qiu X H, Nazin G V and Ho W 2004 *Phys. Rev. Lett.* **92** 206102
[114] Wu S W, Ogawa N and Ho W 2006 *Science* **312** 1362–5
[115] Wu S W, Ogawa N, Nazin G V and Ho W 2008 *J. Phys. Chem.* C **112** 5241–4
[116] Wu S W, Ogawa N, Nazin G V and Ho W 2010 *Phys. Rev.* B **82** 085444
[117] Ogawa N, Mikaelian G and Ho W 2007 *Phys. Rev. Lett.* **98** 166103
[118] Huan Q, Jiang Y, Zhang Y Y, Ham U and Ho W 2011 *J. Chem. Phys.* **135** 014705
[119] Brázdová V, Ganduglia-Pirovanov M V and Sauer J 2010 *J. Phys. Chem.* C **114** 4983–94
[120] Stempel S 1998 Nukleation, Wachstum und Struktur kleiner Metallpartikel auf einer geordneten Aluminiumoxidunterlage *PhD Thesis* Freie Universität Berlin
[121] Bäumer M, Biener J and Madix R J 1999 *Surf. Sci.* **432** 189–98
[122] Hill T, Mozaffari-Afshar M, Schmidt J, Risse T, Stempel S, Heemeier M and Freund H-J 1998 *Chem. Phys. Lett.* **292** 524–30
[123] Bäumer M, Frank M, Heemeier M, Kühnemuth R, Stempel S and Freund H-J 2000 *Surf. Sci.* **454–456** 957–62
[124] Hill T, Risse T and Freund H-J 2005 *J. Chem. Phys.* **122** 164704
[125] Napetschnig E, Schmid M and Varga P 2007 *Surf. Sci.* **601** 3233
[126] Winkler A 2005 Untersuchung der Deposit-Substrat Wechselwirkungen und des Oxidationsverhaltens von Nanopartikeln auf einem oxidischen Träger am Beispiel der Systeme Ni/$Al_{10}O_{13}$/NiAl(110) und Ge/$Al_{10}O_{13}$/NiAl(110) *PhD Thesis* Universität Oldenburg
[127] Bäumer M, Frank M, Libuda J, Stempel S and Freund H-J 1997 *Surf. Sci.* **391** 204–15
[128] Nepijko S, Klimenkov M, Adelt M, Kuhlenbeck H, Schlögl R and Freund H-J 1999 *Langmuir* **15** 5309–13
[129] Nilius N, Ernst N and Freund H-J 2000 *Phys. Rev. Lett.* **84** 3994–7
[130] Nepijko S, Klimenkov M, Kuhlenbeck H, Zemlyanov D, Herein D, Schlögl R and Freund H-J 1998 *Surf. Sci.* **412/413** 192–201
[131] Klimenkov M, Nepijko S, Kuhlenbeck H, Bäumer M, Schlögl R and Freund H-J 1997 *Surf. Sci.* **391** 27–36
[132] Ernst N, Duncombe B, Bozdech G, Naschitzki M and Freund H-J 1999 *Ultramicroscopy* **79** 231–8
[133] Benten W, Nilius N, Ernst N and Freund H-J 2005 *Phys. Rev.* B **72** 045403
[134] Yi C-W and Szanyi J 2009 *J. Phys. Chem.* C **113** 716–23
[135] Handke B, Simonsen J B, Bech M, Li Z and Møller P J 2006 *Surf. Sci.* **600** 5123–30
[136] Uhl A, Sainio J, Lahtinen J, Shaikhutdinov S and Freund H-J 2007 *Surf. Sci.* **601** 5605–10
[137] Magg N, Immaraporn B, Giorgi J B, Schroeder Th, Bäumer M, Döbler J, Wu Z, Kondratenko E, Cherian M, Baerns M, Stair P C, Sauer J and Freund H-J 2004 *J. Catal.* **226** 88–100
[138] Sobota M, Nikiforidis I, Hieringer W, Paape N, Happel M, Steinrück H-P, Görling A, Wasserscheid P, Laurin M and Libuda J 2010 *Langmuir* **26** 7199–207
[139] Sobota M, Schmid M, Happel M, Amende M, Maier F, Steinrück H-P, Paape N, Wasserscheid P, Laurin M, Gottfried J M and Libuda J 2010 *Phys. Chem. Chem. Phys.* **12** 10610–21
[140] Jaeger R M 1992 Adsorptionsuntersuchungen an epitaktisch gewachsenen Al_2O_3/NiAl-Schichten *PhD Thesis* Universität Bochum
[141] Johánek V, Laurin M, Grant A W, Kasemo B, Henry C R and Libuda J 2004 *Science* **304** 1639–44

[142] Schlienz H, Beckendorf M, Katter U J, Risse T and Freund H-J 1995 *Phys. Rev. Lett.* **74** 761–4
[143] Yi C-W and Szanyi J 2007 *J. Phys. Chem.* C **111** 17597–5602
[144] Schauermann S, Hoffmann J, Johánek V, Hartmann J and Libuda J 2002 *Phys. Chem. Chem. Phys.* **4** 3909–18
[145] Pradhan N A, Liu N and Ho W 2005 *J. Phys. Chem.* B **109** 8513–8
[146] Chen Zh, Fujita S and Fukui K i 2011 *J. Phys. Chem.* C **115** 14270–7
[147] Katter U J, Hill T, Risse T, Schlienz H, Beckendorf M, Klüner T, Hamann H and Freund H-J 1997 *J. Phys. Chem.* B **101** 552–60
[148] Katter U J, Hill T, Risse T, Schlienz H, Beckendorf M, Klüner T, Hamann H and Freund H-J 1997 *J. Phys. Chem.* B **101** 3776–80
[149] Haq S, Winkler C, Carew A, Ledieu J and Raval R 2004 *J. Catal.* **226** 1–8
[150] Hoffmann R, Lantz M A, Hug H J, van Schendel P J A, Kappenberger P, Martin S, Baratoff A and Güntherodt H-J 2002 *Appl. Surf. Sci.* **288** 238–44
[151] Albers B, Schwendemann T C, Baykara M Z, Pilet N, Liebmann M, Altman E I and Schwarz U D 2009 *Nature Nanotechnol.* **4** 307–10